

Hierarchical Fusion of Local and Global Visual Features with Mixture-of-Experts for Remote Sensing Image Scene Classification

Yuanhao Tang, Xuechao Zou, Zhengpei Hu, Jianqiang Huang, Junliang Xing, Chengkun Zhang

Abstract—Remote sensing image scene classification remains a challenging task, primarily due to the complex spatial structures and multi-scale characteristics of ground objects. Although CNN-based methods excel at extracting local inductive biases, and Mamba-based approaches demonstrate impressive capabilities in efficiently capturing global sequential context, relying on a single paradigm restricts the model’s ability to simultaneously characterize fine-grained textures and complex spatial structures. To tackle this, we propose a parallel heterogeneous encoder, a hierarchical fusion module designed to achieve effective local-global co-representation. It consists of two parallel pathways: a local visual encoder for extracting multi-scale local visual features, and a global visual encoder for capturing efficient global visual features. The core innovation lies in its hierarchical fusion module, which progressively aggregates multi-scale features from both pathways, enabling dynamic cross-level feature interaction and contextual reconstruction to produce highly discriminative representations. These fused features are then adaptively routed through a mixture-of-experts classifier head, which dynamically dispatches them to the most suitable experts for fine-grained scene recognition. Experiments on AID, NWPU-RESISC45, and UC Merced show that our model achieves 93.72%, 95.54%, and 96.92% accuracy, surpassing SOTA methods with an optimal balance of performance and efficiency. Code is available at <https://anonymous.4open.science/r/classification-41DF>.

Index Terms—Remote sensing images, scene classification, local-global fusion, mixture-of-experts

I. INTRODUCTION

WITH the rapid advancement of Earth observation technologies, high-resolution remote sensing imagery has become increasingly accessible [1]. Covering continuous spectral bands [2], such imagery provides rich spatial and semantic information for applications such as urban mapping and environmental monitoring [3], [4]. Remote sensing image scene classification (RSIC) aims to assign semantic labels to aerial scenes but remains challenging due to complex spatial structures, large-scale variations, and high intra-class diversity.

Recent RSIC methods are dominated by deep learning approaches [5], mainly including convolutional neural networks (CNNs) [6] and Transformer-based models [7], [8]. CNNs excel at modeling local textures and structures but struggle with long-range spatial interactions, while Transformers capture global context at the cost of

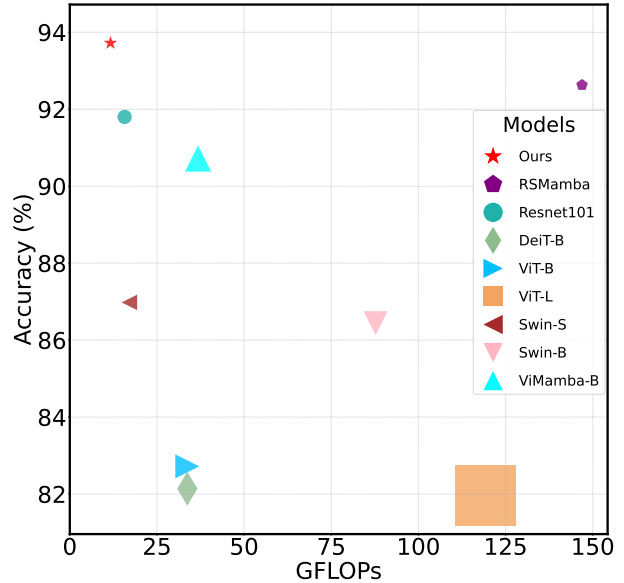


Fig. 1. Accuracy and efficiency comparison. Bubble size denotes parameters. Our method (red star) achieves the optimal balance.

quadratic complexity and may overlook fine-grained local cues.

Recently, Mamba [10], built upon state space models (SSMs) [10], has emerged as an efficient alternative for long-sequence modeling with linear complexity and has been extended to vision tasks [11]. However, existing RSIC approaches often adopt Mamba as a standalone backbone, implicitly assuming that stronger global modeling alone is sufficient, while neglecting the importance of strong local inductive priors.

In contrast, we argue that effective remote sensing scene understanding does not require a heavy global modeling backbone, but rather a lightweight and efficient mechanism to inject global contextual priors into locally discriminative representations. Motivated by this insight, we propose a parallel heterogeneous encoder that explicitly decouples local and global representation learning while maintaining high computational efficiency (see Fig. 1). Specifically, a CNN-based local encoder extracts multi-scale local textures and structural cues, whereas a shallow Mamba-based encoder is deliberately designed as a lightweight global context enhancer, capturing long-

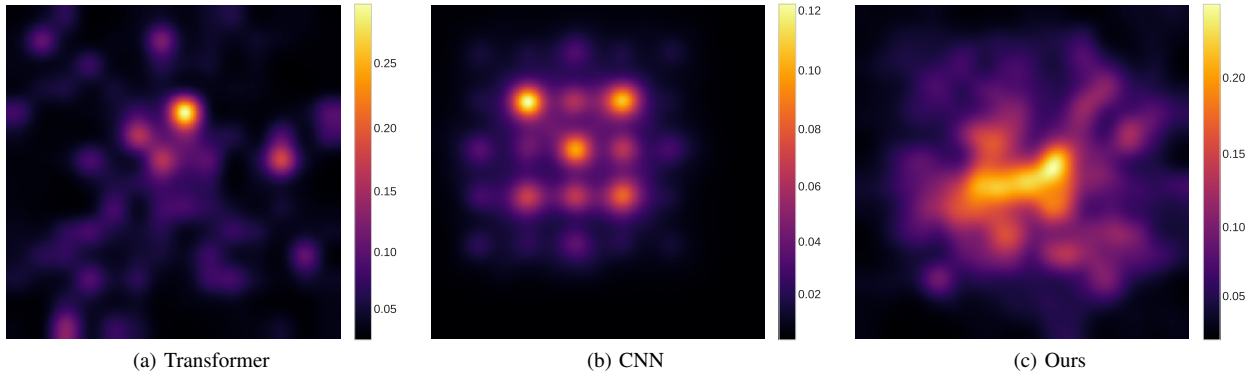


Fig. 2. Effective receptive field (ERF) comparison [9].

range dependencies without overwhelming local feature discrimination.

To bridge the semantic gap between heterogeneous representations, we design a hierarchical fusion module with densely connected dual-attention multi-scale fusion blocks, enabling progressive cross-level feature interaction. Furthermore, to explicitly handle the high intra-class variance inherent in remote sensing scenes, we introduce a mixture-of-experts (MoE) classifier head [12], which enables conditional specialization through dynamic routing with minimal overhead.

The main contributions of this paper are summarized as follows:

- We propose a parallel heterogeneous encoder that synergizes CNN-based local inductive priors with a lightweight Mamba-based global context enhancer for efficient local–global co-representation.
- We design a hierarchical fusion module with dense cross-scale connections to align heterogeneous features and facilitate progressive semantic interaction.
- We introduce a task-aware mixture-of-experts classifier head to address high intra-class variance in remote sensing scene classification.
- Extensive experiments on three benchmarks demonstrate state-of-the-art performance with a favorable accuracy–efficiency trade-off.

II. RELATED WORK

A. Remote Sensing Image Scene Classification

The design of RSIC models has evolved to solve the trade-off between receptive field and efficiency. (1) CNNs [13] lead local feature extraction but are restricted by local receptive fields, limiting long-range dependency modeling. (2) vision transformers (ViTs) [14], [15] capture global context via self-attention but incur quadratic complexity, prompting hybrid designs [16]. (3) Recently, Mamba [10], [17] yields global modeling with linear complexity via selective scanning. This paradigm is now used for remote

sensing [18], offering a robust solution to the limitations of prior arts.

B. Mixture-of-Experts

MoE [19], [20] increases model capacity via conditional computation, where a gating network dynamically selects specialized experts for each input. MoE has demonstrated strong scalability and performance in natural language processing and computer vision tasks [21]. In the remote sensing domain, however, its applications remain relatively limited, primarily focusing on image captioning or multi-task learning scenarios [22].

III. METHOD

We propose a framework to integrate local details with global semantics. As shown in Fig. 3, it comprises a parallel heterogeneous encoder, a hierarchical fusion module, and a mixture-of-experts (MoE) head. First, the local and global visual encoders extract visual features and global sequences, respectively. Next, the central hierarchical fusion module aggregates the extracted features, followed by an MoE head for adaptive classification. Overall, this approach effectively leverages local-global synergy and expert-based decision-making.

A. Parallel Heterogeneous Encoder

As illustrated in Fig. 3, the proposed architecture employs a parallel heterogeneous encoder to extract complementary visual information through two specialized branches: the local visual encoder and the global visual encoder.

1) *Local Visual Encoder*: Built on ResNet, this branch focuses on learning fine-grained local textures. After a Stem module reduces spatial redundancy, features pass through stacked ResNet stage blocks (RSTB). While a standard ResNet backbone traditionally consists of four stages, we selectively extract features from the last three stages to strike an optimal balance between semantic depth and computational cost. These hierarchical outputs are further refined by the local feature enhancement

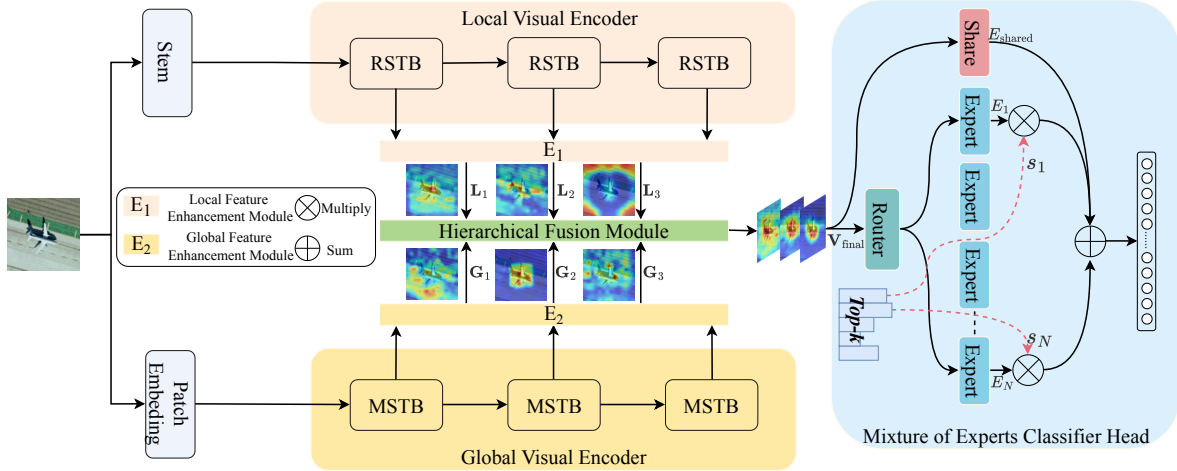


Fig. 3. Architecture of the proposed model. It comprises a parallel local-global visual encoder, a hierarchical fusion module, and a mixture-of-experts classifier head.

module (\mathbf{E}_1) to align their distributions, yielding the enhanced local features $\mathbf{L} = \{\mathbf{L}_i \in \mathbb{R}^{C_i \times H_i \times W_i}\}_{i=1}^3$.

2) *Global Visual Encoder*: Adopting the Vision Mamba backbone, this branch models global context. The hierarchical features are modeled by cascaded mamba stage blocks (MSTB), which leverage SSM to capture global semantic information with linear complexity. Following spatial reshaping to restore 2D structure, the features are further refined by the global feature enhancement module (\mathbf{E}_2). This process yields the enhanced global features $\mathbf{G} = \{\mathbf{G}_i \in \mathbb{R}^{C_i \times H_i \times W_i}\}_{i=1}^3$, serving as the global semantic guidance for the subsequent fusion module.

B. Hierarchical Fusion Module

The hierarchical fusion module (Fig. 4) bridges local and global branches via a top-down aggregation strategy in three steps:

First, local features \mathbf{L}_i are aligned via a 1×1 convolution: $\hat{\mathbf{L}}_i = \text{Conv}_{1 \times 1}(\mathbf{L}_i)$.

Second, the aligned $\hat{\mathbf{L}}_i$ and global features \mathbf{G}_i are fused with upsampled priors from the previous stage to generate the refined feature map $\mathbf{Z}_i \in \mathbb{R}^{C_i \times H_i \times W_i}$:

$$\mathbf{Z}_i = \begin{cases} \text{DB}([\hat{\mathbf{L}}_i, \mathbf{G}_i]), & i = 1 \\ \text{DB}([\hat{\mathbf{L}}_i, \mathbf{G}_i, \text{Up}(\mathbf{Z}_{i-1})]), & i \in \{2, 3\} \end{cases} \quad (1)$$

where $[\cdot]$, $\text{Up}(\cdot)$, and DB denote concatenation, upsampling, and the DAMF-Block, respectively.

Finally, the refined features \mathbf{Z}_i are pooled and flattened into vectors $\mathbf{v}_i \in \mathbb{R}^{C_i}$, which are concatenated into the final representation:

$$\mathbf{V}_{\text{final}} = [\mathbf{v}_1, \mathbf{v}_2, \mathbf{v}_3] \in \mathbb{R}^{C_{\text{total}}}, \quad (2)$$

where $C_{\text{total}} = \sum C_i$. $\mathbf{V}_{\text{final}}$ effectively suppresses background noise and serves as the input for the classifier.

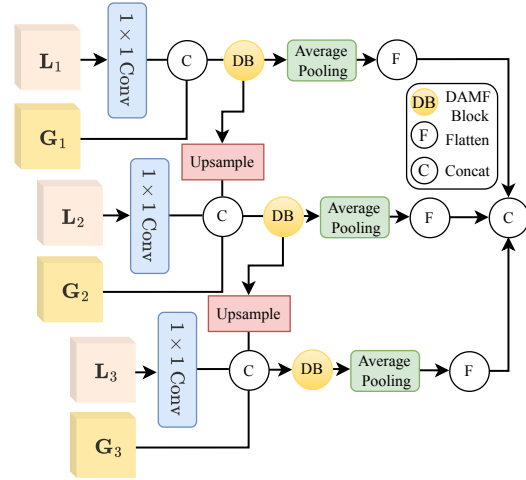


Fig. 4. Details of the proposed hierarchical fusion module.

C. Mixture-of-Experts Classifier Head

To efficiently address high intra-class variance, we employ a MoE head (right panel of Fig. 3) [12]. It comprises a fixed *shared expert* for common patterns and N *routed experts* with dynamic Top- k activation. Given the input $\mathbf{V}_{\text{final}}$, a router generates gating scores $\mathbf{S} \in \mathbb{R}^N$. The output $\mathbf{V}_{\text{out}} \in \mathbb{R}^{C_{\text{total}}}$ sums the shared and weighted selected features:

$$\mathbf{V}_{\text{out}} = \underbrace{E_{\text{shared}}(\mathbf{V}_{\text{final}})}_{\text{Shared Knowledge}} + \underbrace{\sum_{j \in \text{Top-}k(\mathbf{S})} s_j E_j(\mathbf{V}_{\text{final}})}_{\text{Specialized Knowledge}}, \quad (3)$$

where E_{shared} and E_j denote expert functions, and s_j is the normalized weight from \mathbf{S} . To prevent *expert collapse*,

TABLE I. Sota performance comparison on three datasets (Trained from scratch).

Model	UC Merced (%)			AID (%)			NWPU (%)		
	P	R	F1	P	R	F1	P	R	F1
<i>CNN-based Models</i>									
ResNet18 [13]	90.40	90.32	90.22	92.28	92.24	92.22	93.82	93.75	93.75
ResNet50 [13]	91.25	90.95	90.85	92.34	92.26	92.22	94.44	94.40	94.40
ResNet101 [13]	93.93	93.81	93.74	91.87	91.80	91.77	94.80	94.75	94.75
<i>Transformer-based Models</i>									
DeiT-T [23]	85.07	84.44	84.42	80.74	80.72	80.63	83.57	83.57	83.45
DeiT-S [23]	91.90	91.75	91.61	80.98	81.04	80.92	83.12	82.99	82.98
DeiT-B [23]	92.53	92.38	92.34	82.20	82.14	82.05	80.11	80.08	79.98
ViT-B [14]	90.49	90.32	90.18	82.79	82.72	82.54	80.25	80.26	80.16
ViT-L [14]	92.80	92.54	92.42	82.08	81.96	81.84	79.50	79.56	79.46
Swin-T [15]	89.28	88.89	88.88	87.41	87.40	87.35	89.79	89.75	89.72
Swin-S [15]	90.01	89.84	89.72	87.03	86.98	87.03	89.42	89.28	89.28
Swin-B [15]	91.93	91.75	91.66	86.51	86.44	86.37	89.55	89.40	89.41
CMTFNet [16]	94.80	95.04	94.64	93.23	93.01	93.01	94.45	94.35	94.31
<i>Mamba-based Models</i>									
VMamba-T [24]	93.14	92.85	92.81	91.59	90.94	91.10	93.97	93.96	93.94
Vision Mamba-T [11]	83.83	83.81	83.06	79.16	78.94	78.68	89.24	89.02	88.97
Vision Mamba-S [11]	89.62	89.68	89.32	87.77	87.66	87.54	95.23	95.22	95.21
Vision Mamba-B [11]	88.94	89.05	88.82	90.98	90.80	90.72	95.10	95.07	95.06
RSMamba-B [18]	94.14	93.97	93.88	92.02	91.53	91.66	94.87	94.87	94.84
RSMamba-L [18]	95.03	94.76	94.74	92.31	91.75	91.90	95.03	95.05	95.02
RSMamba-H [18]	95.47	95.23	95.25	92.97	92.51	92.63	95.22	95.19	95.18
HC-Mamba-T [25]	94.12	94.59	94.76	91.97	91.47	91.42	94.88	94.96	94.87
HC-Mamba-S [25]	95.10	95.00	95.08	92.33	91.88	91.95	95.10	95.12	95.08
HC-Mamba-B [25]	95.55	95.31	95.34	93.02	92.68	92.86	95.32	95.26	95.25
Ours	96.92	96.83	96.81	93.76	93.72	93.71	95.54	95.52	95.52

we add an auxiliary load-balancing loss \mathcal{L}_{aux} . The total objective is:

$$\mathcal{L}_{\text{total}} = \mathcal{L}_{\text{CE}}(\mathbf{y}, \hat{\mathbf{y}}) + \lambda \mathcal{L}_{\text{aux}}, \quad (4)$$

where \mathcal{L}_{CE} computes the cross-entropy between the ground truth \mathbf{y} and the prediction $\hat{\mathbf{y}}$ (with $\mathbf{y}, \hat{\mathbf{y}} \in \mathbb{R}^{N_{\text{cls}}}$), and we set $\lambda = 0.01$ to regulate the trade-off. \mathcal{L}_{aux} penalizes routing imbalance.

IV. EXPERIMENT

A. Datasets

We evaluate the proposed method on three datasets: UC Merced [3], AID [4], and NWPU-RESISC45 [26]. Varying significantly in scale, resolution, and data volume, these datasets provide a comprehensive assessment of the model’s robustness and generalization capability across diverse scene complexities.

B. Implementation Details

All models are implemented in PyTorch and trained from scratch for 500 epochs on NVIDIA A800 GPUs. We utilize the AdamW [27] optimizer with a batch size of 256, an initial learning rate of 5×10^{-4} , and weight decay of 0.05, modulated by a cosine annealing schedule with linear warm-up. Input images are resized to 224×224 with standard data augmentation (random flipping and

TABLE II. Impact of architecture, fusion strategy, and classifier on aid.

Variant	P (%)	R (%)	F1 (%)
Full Model	93.76	93.72	93.71
<i>Architecture Analysis</i>			
w/o Global Visual Encoder	92.36	92.34	92.33
w/o Local Visual Encoder	88.19	88.16	88.13
<i>Fusion Strategy</i>			
Hierarchical Fusion \rightarrow Concat	91.77	91.74	91.72
Hierarchical Fusion \rightarrow Cross Attention	92.38	92.36	92.33
Hierarchical Fusion \rightarrow AFF [30]	93.15	93.14	93.10
<i>Classifier Analysis</i>			
w/o MoE (use MLP)	93.30	93.25	93.28

color jittering). The objective function is cross-entropy loss with label smoothing ($\epsilon = 0.1$). For evaluation, we report accuracy alongside weighted precision, recall, and F1-score to assess performance.

C. Ablation and Discussion

The impact of the proposed design components is analyzed on the AID dataset.

1) *Impact of Parallel Heterogeneous Encoder*: Table II validates the necessity of our heterogeneous design. Removing the global visual encoder leads to a 1.38% reduction in F1 score, confirming its specific role in capturing long-range global contexts. More critically, eliminating the local visual encoder causes a catastrophic 5.58% drop (plummeting to 88.13%). This sharp decline

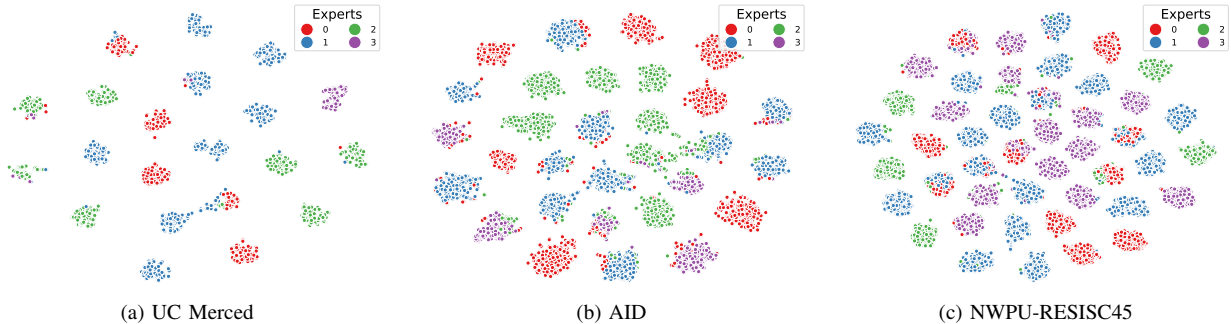


Fig. 5. t-SNE [28] colored by dominant expert. Distinct clusters confirm structured routing.

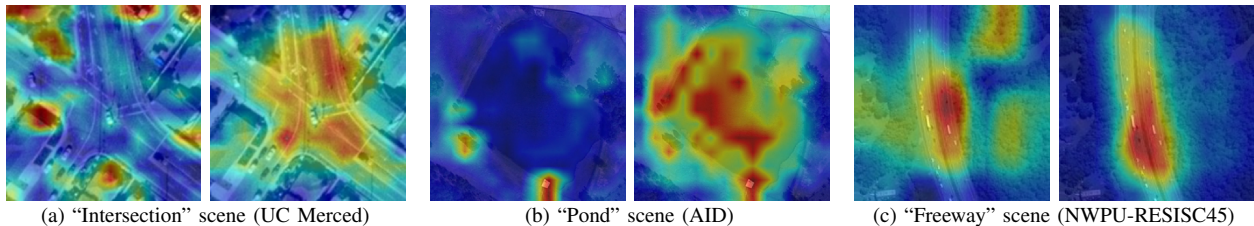


Fig. 6. CAM [29] comparison: ResNet-50 (left) vs. Ours (right).

supports our architectural premise: the global visual encoder serves as a lightweight enhancer rather than a standalone backbone. Due to its shallow depth (10 layers) and low computational footprint, it lacks the independent capacity to model complex patterns and inherently relies on the robust local inductive biases of the local visual encoder. Ultimately, positioning Mamba as an auxiliary branch rather than a deep standalone backbone enables a synergy that yields a more robust representation than heavy single-paradigm architectures.

2) *Component Effectiveness*: As summarized in Table II, we conduct a comprehensive ablation study to validate the proposed fusion strategy and classifier design. For feature fusion, replacing our hierarchical fusion with simple concatenation results in a substantial 1.99% F1 decline, while neither the computation-heavy cross-attention (92.33%) nor the lightweight AFF [30] (93.10%) matches the full model (93.71%). This indicates our mechanism is superior in bridging the semantic gap between local and global visual features compared to generic SOTA modules. Furthermore, replacing the MoE classifier head with a standard MLP causes a discernible performance drop, confirming that dynamic routing effectively addresses the high intra-class variance in remote sensing scenes by adaptively selecting task-specific experts.

3) *Impact of MoE Expert Count*: We analyze how the number of experts N influences performance. Relative to the baseline ($N = 1$), the 4-expert MoE achieves consistent F1 improvements by leveraging dynamic gating for adaptive feature selection. However, as depicted in Fig. 7, scaling N to 8 or 12 incurs higher computational

costs (28.32M params) while performance saturates or degrades due to potential overfitting. These results confirm that $N = 4$ offers the optimal trade-off, ensuring sufficient capacity for diverse scenes while maintaining parameter efficiency.

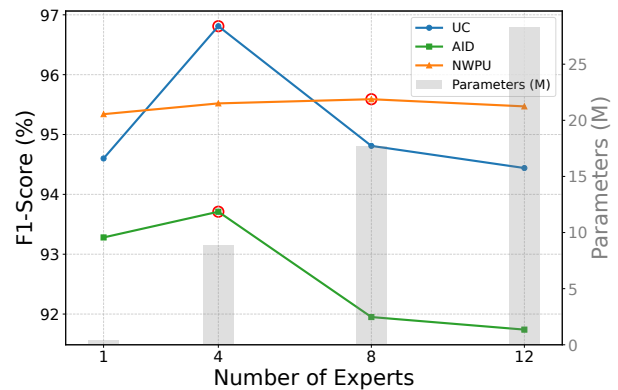


Fig. 7. Performance vs. parameters for varying experts, validating the 4-expert model.

D. Comparison With the State-of-the-Art

1) *Quantitative Analysis*: As shown in Table I, our model establishes new benchmarks across all datasets, surpassing the strongest competitor, CMTFNet, by 1.21% on NWPU. Crucially, as a result of the lightweight design analyzed in the ablation study, our method achieves an optimal accuracy-efficiency trade-off (Fig. 1). It requires over $12\times$ fewer FLOPs (11.67G) than the 24-layer RSMamba (146.92G). These results validate that synergizing local features with a streamlined global

context yields a more robust and efficient representation than heavy single-paradigm or hybrid architectures.

2) *Qualitative Analysis*: Visualization reveals the internal mechanisms of our model. As shown in Fig. 5, t-SNE projections confirm that experts in the MoE module are clearly specialized for different semantic categories through structured routing. Furthermore, Grad-CAM comparisons (Fig. 6) indicate that our model produces more focused and complete activation maps than ResNet-50. These results demonstrate that the hierarchical fusion strategy effectively concentrates attention on core semantic targets while suppressing background noise.

V. CONCLUSION

We present a parallel heterogeneous encoder that synergizes local and global visual features via a hierarchical fusion module and an adaptive MoE head. Extensive experiments across three datasets show that the proposed method achieves state-of-the-art performance with superior computational efficiency, significantly outperforming existing single-paradigm baselines. These results validate the efficacy of our hierarchical fusion strategy. Future work will extend this framework to remote sensing object detection and semantic segmentation tasks.

REFERENCES

- [1] Qiqi Zhu, Weihuan Deng, Zhuo Zheng, Yanfei Zhong, and Deren Li, "A spectral-spatial-dependent global learning framework for insufficient and imbalanced hyperspectral image classification," *IEEE Trans. Cybern.*, 2021.
- [2] Jose M. Bioucas-Dias, Antonio Plaza, Gustavo Camps-Valls, Paul Scheunders, Nasser Nasrabadi, and Jocelyn Chanussot, "Hyperspectral remote sensing data analysis and future challenges," *IEEE Geosci. Remote Sens. Mag.*, vol. 1, no. 2, pp. 6–36, 2013.
- [3] Yi Yang and Shawn Newsam, "Bag-of-visual-words and spatial extensions for land-use classification," in *ACM SIGSPATIAL GIS 2010*, 2010, pp. 270–279.
- [4] Gui-Song Xia, Jingwen Hu, Fan Hu, Baoguang Shi, Xiang Bai, Yanfei Zhong, Liangpei Zhang, and Xiaoqiang Lu, "Aid: A benchmark data set for performance evaluation of aerial scene classification," *TGRS*, vol. 55, no. 7, pp. 3965–3981, 2017.
- [5] Adekanmi Adeyinka Adegun, Serestina Viriri, and Jules-Raymond Tapamo, "Review of deep learning methods for remote sensing satellite images classification: experimental survey and comparative analysis," *Journal of Big Data*, vol. 10, no. 1, pp. 93, 2023.
- [6] Marco Castelluccio, Giovanni Poggi, Carlo Sansone, and Luisa Verdoliva, "Land use classification in remote sensing images by convolutional neural networks," *arXiv preprint arXiv:1508.00092*, 2015.
- [7] Jianrong Zhang, Hongwei Zhao, and Jiao Li, "Trs: Transformers for remote sensing scene classification," *Remote Sensing*, vol. 13, no. 20, pp. 4143, 2021.
- [8] Yakoub Bazi, Laila Bashmal, Mohamad M Al Rahhal, Reham Al Dayil, and Naif Al Ajlan, "Vision transformers for remote sensing image classification," *Remote Sensing*, vol. 13, no. 3, pp. 516, 2021.
- [9] Xiaohan Ding, Xiangyu Zhang, Jungong Han, and Guiguang Ding, "Scaling up your kernels to 31x31: Revisiting large kernel design in cnns," in *CVPR*, 2022, pp. 11963–11975.
- [10] Albert Gu and Tri Dao, "Mamba: Linear-time sequence modeling with selective state spaces," in *First conference on language modeling*, 2024.
- [11] Lianghui Zhu, Bencheng Liao, Qian Zhang, Xinlong Wang, Wenyu Liu, and Xinggang Wang, "Vision mamba: efficient visual representation learning with bidirectional state space model," in *Proc. ICML 2024*, 2024, pp. 62429–62442.
- [12] Aixin Liu, Bei Feng, Bing Xue, Bingxuan Wang, Bochao Wu, Chengda Lu, Chenggang Zhao, Chengqi Deng, Chenyu Zhang, Chong Ruan, et al., "Deepseek-v3 technical report," *CoRR*, 2024.
- [13] Kaiming He, Xiangyu Zhang, Shaoqing Ren, and Jian Sun, "Deep residual learning for image recognition," in *Proc. CVPR*, 2016, pp. 770–778.
- [14] Alexey Dosovitskiy, Lucas Beyer, Alexander Kolesnikov, Dirk Weissenborn, Xiaohua Zhai, Thomas Unterthiner, Mostafa Dehghani, Matthias Minderer, Georg Heigold, Sylvain Gelly, et al., "An image is worth 16x16 words: Transformers for image recognition at scale," in *ICLR*, 2020.
- [15] Ze Liu, Yutong Lin, Yue Cao, Han Hu, Yixuan Wei, Zheng Zhang, Stephen Lin, and Baining Guo, "Swin transformer: Hierarchical vision transformer using shifted windows," in *Proc. ICCV*, 2021, pp. 10012–10022.
- [16] Honglin Wu, Peng Huang, Min Zhang, Wenlong Tang, and Xinyu Yu, "Cmfnnet: Cnn and multiscale transformer fusion network for remote-sensing image semantic segmentation," *TGRS*, vol. 61, pp. 1–12, 2023.
- [17] Kai Li, Guo Chen, and Xiaolin Hu, "Spmamba: State-space model is all you need in speech separation," *arXiv preprint arXiv:2404.02063*, 2024.
- [18] Keyan Chen, Bowen Chen, Chenyang Liu, Wenyuan Li, Zhengxia Zou, and Zhenwei Shi, "Rsmamba: Remote sensing image classification with state space model," *IEEE Geosci. Remote Sens. Lett.*, vol. 21, pp. 1–5, 2024.
- [19] Robert A Jacobs, Michael I Jordan, Steven J Nowlan, and Geoffrey E Hinton, "Adaptive mixtures of local experts," *Neural computation*, vol. 3, no. 1, pp. 79–87, 1991.
- [20] Kai Li and Yi Luo, "Subnetwork-to-go: Elastic neural network with dynamic training and customizable inference," in *ICASSP*, 2024, pp. 6775–6779.
- [21] Carlos Riquelme, Joan Puigcerver, Basil Mustafa, Maxim Neumann, Rodolphe Jenatton, André Susano Pinto, Daniel Keysers, and Neil Houlsby, "Scaling vision with sparse mixture of experts," *Adv. Neural Inf. Process. Syst.*, vol. 34, pp. 8583–8595, 2021.
- [22] Hui Lin, Danfeng Hong, Shuhang Ge, Chuyao Luo, Kai Jiang, Hao Jin, and Congcong Wen, "Rs-moe: A vision-language model with mixture of experts for remote sensing image captioning and visual question answering," *TGRS*, 2025.
- [23] Hugo Touvron, Matthieu Cord, Matthijs Douze, Francisco Massa, Alexandre Sablayrolles, and Hervé Jégou, "Training data-efficient image transformers & distillation through attention," in *Proc. ICML*. PMLR, 2021, pp. 10347–10357.
- [24] Yue Liu, Yunjie Tian, Yuzhong Zhao, Hongtian Yu, Lingxi Xie, Yaowei Wang, Qixiang Ye, Jianbin Jiao, and Yunfan Liu, "Vmamba: visual state space model," in *NeurIPS 2024*, 2024, pp. 103031–103063.
- [25] Mo Yang and Luo Chen, "Hc-mamba: Remote sensing image classification via hybrid cross-activation state space model," *IEEE J. Sel. Top. Appl. Earth Obs. Remote Sens.*, 2025.
- [26] Gong Cheng, Junwei Han, and Xiaoqiang Lu, "Remote sensing image scene classification: Benchmark and state of the art," *Proceedings of the IEEE*, vol. 105, no. 10, pp. 1865–1883, 2017.
- [27] Ilya Loshchilov and Frank Hutter, "Decoupled weight decay regularization," in *ICLR*, 2019.
- [28] Laurens Van der Maaten and Geoffrey Hinton, "Visualizing data using t-sne," *Journal of machine learning research*, vol. 9, no. 11, 2008.
- [29] Ramprasaath R. Selvaraju, Michael Cogswell, Abhishek Das, Ramakrishna Vedantam, Devi Parikh, and Dhruv Batra, "Grad-CAM: Visual explanations from deep networks via gradient-based localization," in *ICCV*, 2017, pp. 618–626.
- [30] Yimian Dai, Fabian Gieseke, Stefan Oehmcke, Yiquan Wu, and Kobus Barnard, "Attentional feature fusion," in *WACV*, 2021, pp. 3559–3568.